Circular geodesics and accretion disks in the Janis-Newman-Winicour and gamma metric spacetimes

Anirban N. Chowdhury,[*] Mandar Patil,[†] Daniele Malafarina,[‡] and Pankaj S. Joshi[§]

Tata Institute of Fundamental Research, Homi Bhabha Road, Colaba, Mumbai 400005, India
(Received 12 December 2011; published 21 May 2012)

We study here circular timelike geodesics in the Janis-Newman-Winicour and Gamma metric space-times which contain a strong curvature naked singularity and reduce to the Schwarzschild metric for a specific value of one of the parameters. We show that for both the metrics the range of allowed parameters can be divided into three regimes where structure of the circular geodesics is qualitatively different. It follows that the properties of the accretion disks around such naked singularities can be significantly different from those of disks around black holes. This adds to previous studies showing that if naked singularities exist in nature, their observational signature would be significantly different from that of the black hole.

I. INTRODUCTION

One of the most important unresolved problems in general relativity, and an issue that has far reaching observational implications, is that of the final fate of complete gravitational collapse of a massive body such as a star.

The Israel-Carter conjecture asserts that a Kerr black hole, which is described by two parameters, namely, mass and angular momentum, would be formed as the endstate of any generic complete gravitational collapse, and thus all other information regarding the nature of the matter fields, symmetries, and initial conditions will be radiated away in the process of collapse. The above statement remains at the stage of conjecture as of now because proving it analytically or numerically is turning out to be a very difficult task. We also do not understand very well how matter would behave at energies beyond nuclear energy scales all the way up to Planck scale as we have no theoretical understanding of evolution of the equation of state of matter at such energies. Thus theoretical studies do not provide a definite answer to the question whether or not black holes are the only possible outcomes of gravitational collapse.

In fact, in the last few years new theoretical models and observations seem to suggest that the true nature of the process could be more complicated. Investigations of gravitational collapse of various matter configurations in the context of the general theory of relativity over the last couple of decades have revealed that the endstates of complete gravitational collapse could either be black holes or naked singularities [1].

Therefore, it is natural to ask the question of what happens during a realistic collapse of a massive body and what will be the endstate of such a collapse. The possibilities can be divided into three main categories:

(i) The body radiates away all higher multipole moments and all asymmetry, thus forming a Kerr black hole.

(ii) Collapse will halt before all matter is squeezed into a spacetime singularity, thus creating a finite sized final object that is different from a black hole.

(iii) Matter will fall into the final spacetime singularity preserving its symmetry structure, thus creating a final configuration in the form of vacuum spacetime with a singularity (that can be covered or naked).

The analytical solutions describing dynamical collapse of a rotating body away from spherical symmetry are few and not well understood at present. Therefore a possible mechanism to account for the first hypothesis is still missing. For this reason it seems natural to turn the attention to the other two options. Ideas following the second hypothesis have been proposed [2], but the nature of these objects and the physical processes that could lead to the formation of the same are not well understood. Furthermore recently some new scenarios have been proposed that include the possibility that gravitational collapse can asymptotically halt, leading to the formation of static configurations of matter that may or may not contain a naked singularity and which could be either finite or infinite in extent [3].

On the other hand, if black holes and naked singularities which are hypothetical astrophysical objects occur in nature, a question would be how they would be observationally different. Therefore some researchers have started looking into the observational features that would distinguish these entities. Black holes and naked singularities could have rather different properties and this could also possibly shed some light on the nature of existing sources, like the supermassive dark objects that dwell at the center of galaxies. Recent studies of gravitational lensing (see for example [4]) and accretion disks (see [3,5–7]) have

---
[*]a.chowdhury@iiserpune.ac.in
[†]mandarp@tifr.res.in
[‡]daniele.malafarina@polimi.it
[§]psj@tifr.res.in

brought out interesting characteristic differences for these objects which could possibly distinguish them from each other. Recently it was also suggested by some of us that ultrahigh energy collisions and fluxes of the escaping collision products could be used for this purpose in certain situations [8].

In the present paper, we investigate the properties of circular geodesics and accretion disks in two spacetimes that arise naturally while generalizing the Schwarzschild solution. One is the Janis-Newman-Winicour (JNW) solution and the other one is the so called Gamma metric (γ-metric henceforth).

The Schwarzschild metric is the unique vacuum solution to Einstein equations under spherical symmetry which is static and asymptotically flat. Different metrics can be obtained from the Schwarzschild solution by relaxing one or more of the assumptions above. Firstly, relaxing the spherical symmetry, we can consider either a static deformation keeping the axial symmetry intact, or we could invoke a spin. One of the solutions that can be obtained in the former case is the γ-metric [9], whereas the spacetime in the latter case is described by the Kerr metric. On the other hand, the assumption of empty spacetime can be relaxed by invoking the presence of either an electromagnetic field or a scalar field. In the former case one obtains the Reissner-Nordström solution, whereas in the latter case, by invoking a massless scalar field, the JNW solution is obtained [10].

The uniqueness theorems give a privileged status to the Kerr and Schwarzschild spacetimes. Nevertheless, since we do not know if in a realistic physical scenario those will necessarily be the resulting metrics, it is of interest to study spacetimes such as JNW and the γ-metric that depart from the black hole models and see if they can be observationally different from their black hole counterparts. The main point that makes the γ-metric and the JNW-metric more appealing is that they are continuously connected to the Schwarzschild solution via the value of one parameter. By reducing this parameter to a specific value we recover exactly the Schwarzschild solution. The interesting point is that the Schwarzschild metric has a black hole whereas these two generalizations contain naked singularities, and therefore we can directly compare the results obtained for models of accretion disks in these metrics with the Schwarzschild case. Furthermore the parameters appearing in the JNW and γ-metric have a clear and direct physical interpretation, as one represents the addition of a scalar field while the other represents an axial deformation.

The first step towards the study of accretion disks is understanding the circular geodesics in the equatorial plane of the spacetime. The study of circular geodesics in Kerr and Reissner-Nordström spacetimes containing black holes or naked singularities depending on the values of the spin and charge parameters, respectively, was recently carried out in [6]. In this paper we investigate the structure of circular geodesics for the JNW and γ spacetimes.

We find that the properties of accretion disks can be divided in three regimes according to the values assumed by a parameter in the solutions. In one regime, the stable circular geodesics extend all the way up to singularity; in the second, the stable circular orbits can exist in two disjoint disks separated by a gap, one disk extending from singularity to a finite radius and another extending from a larger radius to infinity. Finally, in the third case a photon sphere surrounds the singularity, and stable circular geodesics can exist from a particular radius above photon sphere to infinity.

II. CIRCULAR EQUATORIAL GEODESICS IN THE JNW METRIC

In this section we investigate the structure of the circular geodesics in the JNW spacetime. As mentioned earlier, the JNW metric is obtained as an extension of the Schwarzschild spacetime when a massless scalar field is present. In a naive sense, the black hole event horizon, *i.e.* a coordinate singularity in the Schwarzschild spacetime transforms to a real physical singularity which is naked. The JNW metric depends upon two parameters, one related to the mass and an additional parameter which can be interpreted as the strength of the scalar field or "scalar charge".

The JNW metric can be written in the following way

$$ds^2 = -A dt^2 + A^{-1} dr^2 + B d\Omega^2, \tag{1}$$

where $d\Omega^2 = d\vartheta^2 + \sin^2\theta d\phi^2$ is the line element of a unit two-sphere and the functions $A(r)$ and $B(r)$ are given by the following expressions

$$A(r) = \left[\frac{2r - r_0(\mu - 1)}{2r + r_0(\mu + 1)}\right]^{(1/\mu)}, \tag{2}$$

$$B(r) = \frac{1}{4}\frac{[2r + r_0(\mu + 1)]^{(1/\mu)+1}}{[2r - r_0(\mu - 1)]^{(1/\mu)-1}}. \tag{3}$$

The two parameters mentioned above are r_0 (that is related to the mass) and the scalar charge μ. The range of μ is given by $\mu \in (1, \infty)$ and the scalar field is given by the following expression,

$$\varphi = \frac{a}{\mu} \ln \left| \frac{2r - r_0(\mu - 1)}{2r + r_0(\mu + 1)} \right|, \tag{4}$$

where μ and a are linked by the relation $\mu = (1 + 8\pi\frac{4a^2}{r_0^2})$. The JNW spacetime contains a strong curvature singularity which is globally naked at

$$r_{\text{sing}} = \frac{1}{2} r_0(\mu - 1), \tag{5}$$

for $\mu \neq 1$.

The Schwarzschild solution in the usual form can be recovered from the JNW solution when $\mu = 1$ after a simple coordinate transformation of the radial coordinate given by $\bar{r} = r + r_0$, with $r_0 = 2M$ which is the usual Schwarzschild radius of the event horizon (note that the radial coordinate r of the JNW metric when $\mu = 1$ does not correspond to the usual Schwarzschild coordinate $\bar{r}$), and where M is related to the total mass of the central body as measured by observers at infinity. Therefore the case where μ is close to 1 corresponds to the small deviations from the Schwarzschild metric due to the presence of a small massless scalar field, whereas large values of μ correspond to the large deviations from the Schwarzschild geometry [11].

A. Geodesics in JNW spacetime: basic equations

We now investigate the structure of timelike equatorial geodesics in the JNW spacetime. The JNW metric is spherically symmetric and static and therefore admits the two Killing vectors $\xi_t = \partial_t$ and $\xi_\phi = \partial_\phi$. As a consequence we have the following conserved quantities along geodesic motion.

$$E = -g_{\alpha\beta}\xi_t^\alpha u^\beta = A(r)U^t, \quad (6)$$

$$L = g_{\alpha\beta}\xi_\phi^\alpha u^\beta = B(r)U^\phi, \quad (7)$$

where $U^\alpha = (U^t, U^r, U^\theta, U^\phi)$ is the four-velocity of the test particle. The constants of motion E and L can be interpreted as the conserved energy and orbital angular momentum per unit mass of the particle, respectively.

Spherical symmetry implies that the motion of the particle will be restricted to a plane which can be chosen by gauge freedom to be the equatorial plane. Thus we set $\theta = \frac{\pi}{2}$ and $U^\theta = 0$.

From Eqs. (6) and (7) using the normalization condition for the four-velocity $U^\alpha U_\alpha = -1$, we obtain the equation for the motion of a particle in the radial direction.

$$\dot{r}^2 + V^2 = E^2. \quad (8)$$

Here V can be thought of as an effective potential for the test particle and it is given by a following expression,

$$V^2 = A(r)\left(1 + \frac{L^2}{B(r)}\right). \quad (9)$$

B. Circular geodesics

From the analysis of the above effective potential we can obtain the structure of circular geodesics. A particle orbiting along a circular geodesics must obey the conditions

$$U^r = \dot{U}^r = 0, \quad (10)$$

as r must stay constant. Here the dot denotes a derivative with respect to the affine parameter for geodesic *i.e.* the proper time.

From Eqs. (8) and (10) it follows that for circular geodesics

$$V = E, \quad \text{and} \quad \frac{\partial V}{\partial r} = 0. \quad (11)$$

Further, one needs to ensure that the circular orbit is stable against small perturbations in the radial direction, and this implies that for a stable orbit the effective potential must admit a minimum:

$$\frac{\partial^2 V}{\partial r^2} > 0. \quad (12)$$

When the effective potential admits a maximum, i.e., when $\frac{\partial^2 V}{\partial r^2} < 0$ the orbit is unstable against small perturbations. The condition for the marginally stable orbit is $\frac{\partial^2 V}{\partial r^2} = 0$, corresponding to the inflection point for the effective potential.

Imposing the conditions (11) on (9) we get the expression for the conserved energy and momentum of the particle orbiting along the geodesic of radius r as

$$L^2 = \frac{r_0}{4(2r - r_0)}\frac{[2r + r_0(\mu + 1)]^{(1/\mu)+1}}{[2r - r_0(\mu - 1)]^{(1/\mu)-1}}, \quad (13)$$

$$E^2 = \frac{2r}{2r - r_0}\left[\frac{2r - r_0(\mu - 1)}{2r + r_0(\mu + 1)}\right]^{(1/\mu)}, \quad (14)$$

from which it follows that we must have

$$r > \frac{r_0}{2} = M, \quad (15)$$

for the energy and angular momentum to be real. Thus the circular geodesics can exists only for those values of r for which this condition holds. The energy and angular momentum diverge at the radius

$$r_{\text{ph}} = \frac{r_0}{2}, \quad (16)$$

which represents the radius at which photons move on circular trajectories and it is known as photon sphere. The photon sphere plays a crucial role in the study of gravitational lensing since its presence delimits a boundary below which lensing effects cannot be observed, therefore implying that two spacetimes that possess a photon sphere at the same radius cannot be distinguished by the observation of lensing effects even though their compact sources might be different.

Imposing the condition for the stability of the circular geodesics against small perturbations along the radial direction in Eq. (9) we get

$$4r^2 - 8rr_0 + r_0^2(\mu^2 - 1) > 0, \quad (17)$$

which implies that the radius of the stable orbit must satisfy the following condition

$$r > r_+ \quad \text{or} \quad r < r_-, \quad (18)$$

where

$$r_\pm = r_0 \left(1 \pm \frac{1}{2}\sqrt{5 - \mu^2} \right). \tag{19}$$

The marginally stable orbits are located at these two values of the radii.

In Fig. 1 are shown the values of the radial coordinates for the singularity, photon sphere, r_+ and r_- depending upon the parameter μ. Three distinct ranges of the parameters emerge where the structure of the circular geodesics will be qualitatively different, namely $\mu \in (1, 2)$, $\mu \in (2, \sqrt{5})$, $\mu \in (\sqrt{5}, \infty)$. We discuss these cases separately.

The conserved energy and angular momentum for test particles as a function of the radius of the circular orbit are plotted in Figs. 2 and 3 respectively, for different values of the parameter μ. The qualitative behavior of these functions is also manifestly different in the three regimes of the parameter mentioned above.

1. Case $\mu \in (1, 2)$

For this range of parameters we have the following relation, as seen from Fig. 1,

$$r_+ > r_{\text{ph}} > r_{\text{sing}} > r_-. \tag{20}$$

This implies that r_- does not exist and a photon sphere covers the singularity. The stable circular orbits can exist in the region given by,

$$r \in (r_+, \infty), \tag{21}$$

which is above the photon sphere. Unstable circular orbits can exist between the photon sphere and r_+ and no circular orbits can exists below the photon sphere up to the singularity.
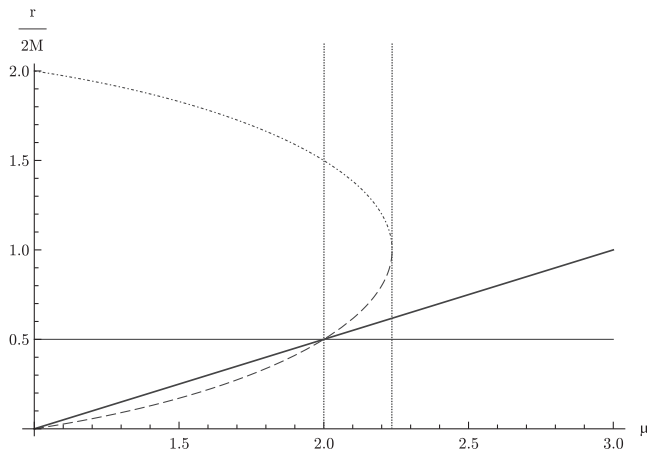

FIG. 1. The value of the radial coordinate (in units of $\frac{1}{2M}$) for the singularity (thick line), photon sphere (thin line), r_+ (dotted and dashed line) and r_- (dashed line) as functions of the parameter μ. It is clear that the structure of the circular geodesics will be qualitatively different in the three different ranges of the parameter, namely, $(1, 2)$, $(2, \sqrt{5})$ and $(\sqrt{5}, \infty)$.
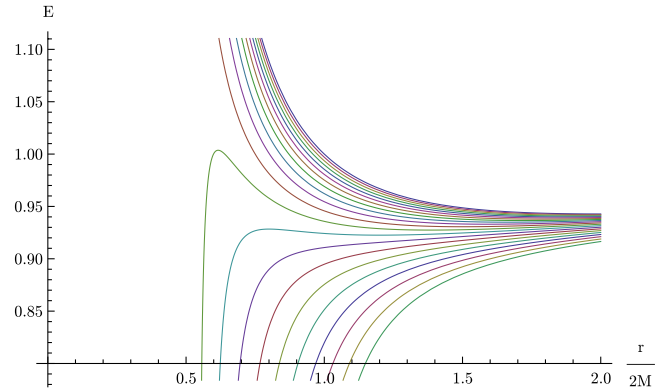

FIG. 2 (color online). The conserved energy per unit mass E is plotted against the radius of the circular orbit r (in units of $\frac{1}{2M}$) for different values of μ. The curves located higher in the diagram correspond to lower values of μ and vice versa. For values of $\mu \in (1, 2)$, E decreases with the decreasing r, attains a minimum and again increases to become infinite before the singularity is reached. For values of $\mu \in (2, \sqrt{5})$, E initially decreases with decreasing r, attains a minimum followed by a maximum and decreases to a zero value at the singularity. Whereas for large values of $\mu \in (\sqrt{5}, \infty)$, E is monotonically decreasing with decreasing r and takes a zero value at the singularity.

In Fig. 4 the general behavior of the effective potential is shown as a function of the radius for a fixed value of the parameter μ in the range considered and for different values of the angular momentum L. The effective potential admits one maximum and one minimum which correspond to the unstable and stable circular orbits, respectively. The
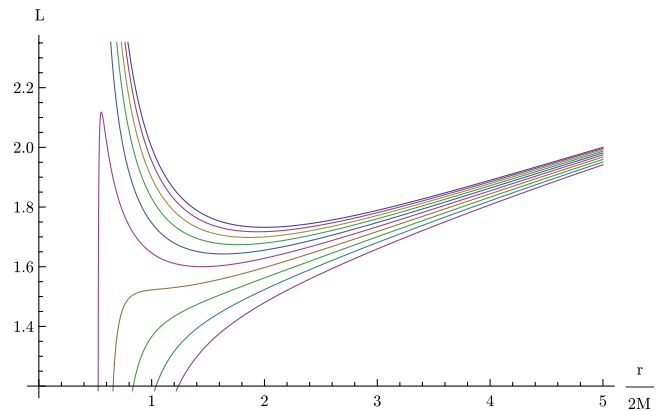

FIG. 3 (color online). The conserved angular momentum per unit mass L is plotted against the radius of the circular orbit r (in units of $\frac{1}{2M}$) for different values of μ. The curves located higher in the diagram correspond to lower values of μ and vice versa. For values of $\mu \in (1, 2)$, L has a minimum at a finite r and increases diverging as the singularity is approached and as r goes to infinity. For values of $\mu \in (2, \sqrt{5})$ L vanishes at the singularity and has a local maximum and a local minimum before increasing indefinitely as r goes to infinity. Whereas for large values of $\mu \in (\sqrt{5}, \infty)$, L increases monotonically from zero at the singularity to infinity as r goes to infinity.
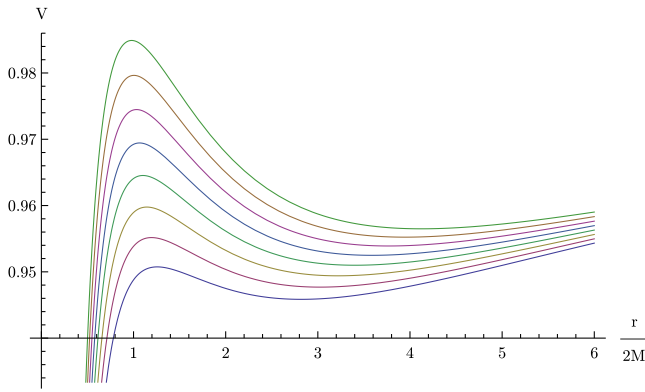
FIG. 4 (color online). The effective potential for radial motion V is plotted as a function of radial coordinate $\frac{r}{2M}$ for $\mu = 1.5 \in (1, 2)$ for different values of L. It can be seen that the V admits one minimum and one maximum, which corresponds to stable and unstable circular orbits, respectively.

FIG. 5 (color online). The effective potential for radial motion V is plotted as a function of radial coordinate $\frac{r}{2M}$ for $\mu = 2.1 \in (2, \sqrt{5})$ for different values of L. It can be seen that V admits two minima and one maximum in between, which indicate the presence of two regions with stable circular orbits separated by one region of unstable circular orbits.

unstable circular orbits lie in the region between the photon sphere and r_+.

Note that both $E(r)$ and $L(r)$ become infinite at a certain finite radius r in this case (as can be seen from Figs. 2 and 3). As we approach the singularity from infinity, the stable circular geodesics can exist up to the minimum of energy and angular momentum. The unstable orbits exist in the region between the minimum and the radial value where $E(r)$ and $L(r)$ blow up, which is the photon sphere. No circular orbits can exist below the photon sphere, a result that is consistent with the earlier discussion.

2. Case $\mu \in (2, \sqrt{5})$

In this range of parameters we get the following relation

$$r_+ > r_- > r_{\text{sing}} > r_{\text{ph}}. \tag{22}$$

This implies that the photon sphere does not exist and there are two distinct regions where circular geodesics can exist, namely,

$$r \in (r_+, \infty) \quad \text{and} \quad r \in (r_{\text{sing}}, r_-). \tag{23}$$

A new interesting feature arises in this case since the second region extends all the way up to singularity. Particles reaching the innermost boundary of the exterior accretion disk would plunge in the region of unstable orbits to reach r_- where they would shock and circularize again, inspiralling onto the singularity.

In Fig. 5 the general behavior of the effective potential for this range of the parameter is shown for different values of L. The effective potential admits two minima which correspond to the two stable circular orbits in the two regions we discussed above. There is also one local maximum between the two minima, which lies in the unstable region between the two stable ones.
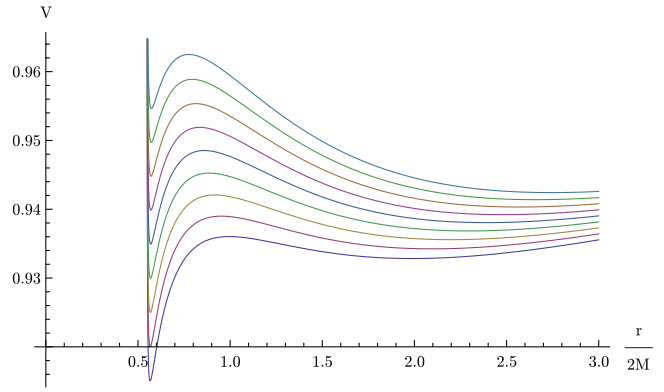
The qualitative behavior of the functions $E(r)$ and $L(r)$ in this range of parameter shows that both quantities do not blow up, instead as r decreases they reach a maximum and then decrease to zero as singularity is approached (see Figs. 2 and 3). The existence of two regions where stable circular geodesics can exist can be derived also from the analysis of $E(r)$ and $L(r)$ as the two regions correspond to the portions where the two functions decrease with the decreasing r, namely, from infinity to the first minimum and from the maximum to the singularity. Since the two functions do not blow up at any allowed radius, no photon sphere is present in the spacetime.

3. Case $\mu \in (\sqrt{5}, \infty)$

Within this range of values for the parameter r_+ and r_- do not exist as the solutions of Eq. (19) are not real. For this range of parameters we have

$$r_{\text{sing}} > r_{\text{ph}}, \tag{24}$$

from which we see that the photon sphere is not present as well. This implies that the stable circular orbits can exist for

$$r \in (r_{\text{sing}}, \infty), \tag{25}$$

i.e. from the singularity to infinity everywhere on the equatorial plane.

In Fig. 6 the general behavior of the effective potential for this range of parameter values for various angular momenta is shown. The effective potential admits only one minimum which indicates the presence of stable circular orbit. Since the potential does not admit maximum, unstable circular orbits do not exists. The circular orbits exist all the way up to the singularity.

In this case, the qualitative behavior of the functions $E(r)$ and $L(r)$ is decreasing from infinity until they become
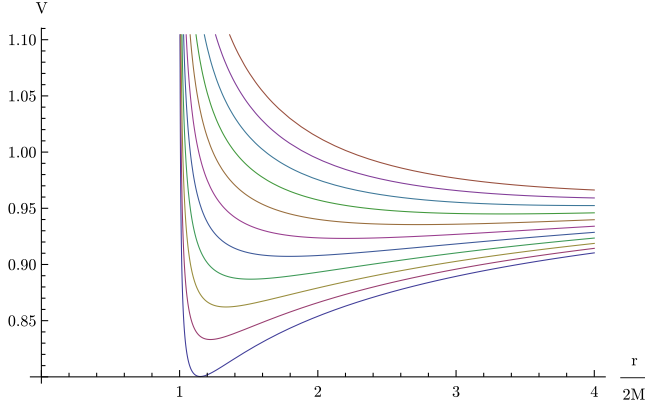
FIG. 6 (color online). The effective potential for radial motion V is plotted against r (in units of $\frac{1}{2M}$) for $\mu = 3 \in (\sqrt{5}, \infty)$ for different values of L. The effective potential admits only one minimum. Unstable orbits do not exists since V does not admit maximum.

zero at the singularity (see Figs. 2 and 3). This implies that the stable circular orbits would exist all the way up to singularity, which is consistent with the above discussion.

III. CIRCULAR EQUATORIAL GEODESICS IN THE GAMMA METRIC

In this section, we study the structure of circular geodesics in the γ spacetime. The γ-metric is obtained by extending the Schwarzschild spacetime when spherical symmetry is deformed to develop a prolate or oblate spheroid.

The γ-metric is a two parameter family of spacetimes belonging to the Weyl class of static, axially symmetric, vacuum solutions of Einstein equations that are asymptotically flat. In principle all the metrics belonging to the Weyl class are known since there is a one to one correspondence between such spacetimes and solutions of the Laplace equation in flat two-dimensional space. The interesting feature of the γ-metric is that it is continuously linked to the Schwarzschild metric via one of the parameters. The two parameters can be defined as a mass parameter M and the parameter γ, that quantifies the deformation from spherical symmetry. We investigate the circular geodesics in γ-spacetime as a function of the deformation parameter.

The γ-metric is given by

$$ds^2 = -Fdt^2 + F^{-1}[Gdr^2 + Hd\theta^2 + (r^2 - 2mr)\sin^2\theta d\phi^2], \tag{26}$$

where the functions $F(r)$, $G(r, \theta)$ and $H(r, \theta)$ are given by the following expressions

$$F = \left(1 - \frac{2M}{r}\right)^\gamma, \tag{27}$$

$$G = \left(\frac{r^2 - 2Mr}{r^2 - 2Mr + M^2\sin^2\theta}\right)^{\gamma^2-1}, \tag{28}$$

$$H = \frac{(r^2 - 2Mr)^{\gamma^2}}{(r^2 - 2Mr - M^2\sin^2\theta)^{\gamma^2-1}}. \tag{29}$$

The total ADM mass as measured by an observer at infinity associated with the γ-spacetime is given by $M_{\text{tot}} = \gamma M$ and the range of the deformation parameter is over all the positive real numbers with the Schwarzschild spacetime recovered when $\gamma = 1$, whereas $\gamma > 1$ ($\gamma < 1$) corresponds to an oblate (prolate) geometry, respectively. In the limit $\gamma = 0$ a flat spacetime is obtained.

There is a strong curvature singularity in the γ spacetime whenever $\gamma \neq 1$ and it is located at the radial value

$$r_{\text{sing}} = 2M. \tag{30}$$

The singularity is visible to all observers if $\gamma < 1$ while for $\gamma > 1$ it has a directional behavior being visible only to observers not on the polar plane. So if we confine ourselves to the equatorial plane, the singularity is a naked singularity [12].

A. Geodesics in γ-spacetime: basic equations

The complete structure of geodesic motion in the γ-metric was studied by Herrera *et al.* [13]. The γ-metric is axially symmetric and static. Thus as in the case of JNW metric the existence of the Killing vectors $\xi_t = \partial_t$ and $\xi_\phi = \partial_\phi$ implies that the following two quantities are constants of motion

$$E = -g_{\alpha\beta}\xi_t^\alpha U^\beta = FU^t, \tag{31}$$

$$L = g_{\alpha\beta}\xi_\phi^\alpha U^\beta = \frac{r^2 - 2Mr}{F}U^\phi, \tag{32}$$

where $U^\alpha = (U^t, U^r, U^\theta, U^\phi)$. We assume that the geodesics are confined to the equatorial plane and thus impose $\theta = \frac{\pi}{2}$.

Using the condition for the normalization of velocity $U^\alpha U_\alpha = -1$ and Eqs. (31) and (32) the equation for the radial motion can be written as

$$G\dot{r}^2 + V^2 = E^2, \tag{33}$$

where V can be thought of as an effective potential and it is given by the following expression

$$V^2 \equiv F + \frac{L^2F^2}{r^2 - 2Mr}. \tag{34}$$

B. Circular geodesics

As described in the previous section the conditions for the circular geodesic are given by

$$U^r = \dot{U}^r = 0, \tag{35}$$

where the dotted quantity means derivative with respect to the affine parameter, *i.e.* the proper time. These again are equivalent to

$$V = E, \quad \text{and} \quad \frac{\partial V}{\partial r} = 0, \tag{36}$$

meaning that the effective potential must be equal to the energy and it must admit an extremum.

For the circular orbits to be stable against radial perturbations the effective potential must admit a minimum, thus satisfying the condition

$$\frac{\partial^2 V}{\partial r^2} > 0. \tag{37}$$

For the unstable circular geodesics we have $\frac{\partial^2 V}{\partial r^2} < 0$, whereas for the marginally stable case we get $\frac{\partial^2 V}{\partial r^2} = 0$.

Now imposing condition (36) on the effective potential (34) we obtain the following expressions for angular momentum and energy

$$L^2 = \left(1 - \frac{2M}{r}\right)^{1-\gamma} \frac{r^2 M \gamma}{r - M(1 + 2\gamma)}, \tag{38}$$

$$E^2 = \left(1 - \frac{2M}{r}\right)^{\gamma} \frac{r - M(1 + \gamma)}{r - M(1 + 2\gamma)}. \tag{39}$$

Circular orbits exist if the condition $r \geq M(1 + 2\gamma)$ is satisfied which ensures that E and L are real.

Conserved energy and angular momentum blow up at the radius of the photon sphere which is given by the equation

$$r_{\text{ph}} = M(1 + 2\gamma). \tag{40}$$

The condition for the stability of the circular geodesics is then

$$r > r_+ \quad \text{or} \quad r < r_-, \tag{41}$$

where

$$r_{\pm} = M(1 + 3\gamma \pm \sqrt{5\gamma^2 - 1}), \tag{42}$$

are the radii of marginally stable orbits.

In Fig. 7 are shown the values of radial coordinate for the singularity, photon sphere, r_+ and r_- as the parameter γ is varied. Three distinct ranges of the parameters emerge where the structure of the circular geodesics will be qualitatively different, namely $\gamma \in (0, \frac{1}{\sqrt{5}})$, $\gamma \in (\frac{1}{\sqrt{5}}, \frac{1}{2})$ and $\gamma \in (\frac{1}{2}, \infty)$. We discuss these cases separately.

The conserved energy and angular momentum as functions of the radius of the orbit of the test particle are plotted in Figs. 8 and 9 respectively for different values of the parameter γ. The qualitative behavior of these functions is also manifestly different in the three regimes of the parameter mentioned above.
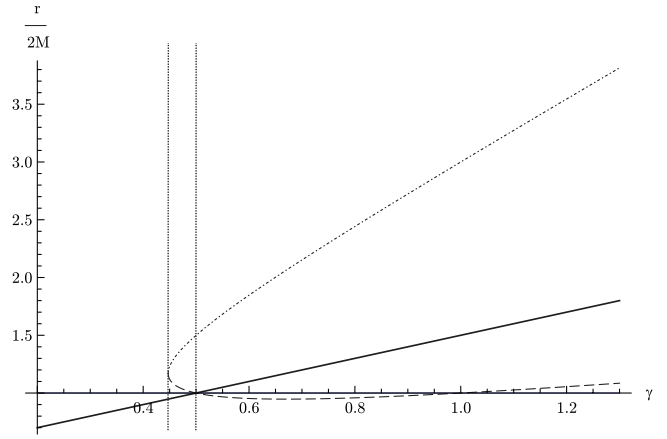

FIG. 7 (color online). The radial curves (in units of $\frac{1}{2M}$) for the singularity (*x*-axis), photon sphere (thick line), r_+ (dotted and dashed line) and r_- (dashed line), respectively, as functions of the parameter γ. It is obvious from the graphs that the structure of the circular geodesics will be qualitatively different in the three different regimes of the parameter, namely $(0, \frac{1}{\sqrt{5}})$, $(\frac{1}{\sqrt{5}}, \frac{1}{2})$ and $(\frac{1}{2}, \infty)$.

1. Case $\gamma \in (0, \frac{1}{\sqrt{5}})$

In this range of parameter r_+ and r_- do not take real values and we have

$$r_{\text{sing}} > r_{\text{ph}}, \tag{43}$$

meaning also that the photon sphere does not exist. This implies that the stable orbits can exist from infinity to the singularity:
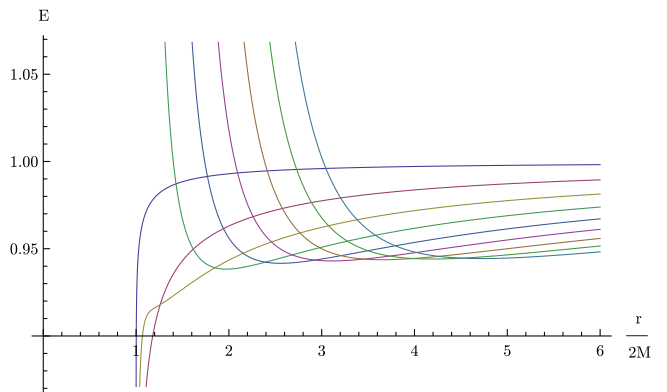

FIG. 8 (color online). The conserved energy per unit mass E is plotted against the radius of the circular orbit r (in units of $\frac{1}{2M}$) for different values of γ. The curves located higher in the diagram correspond to higher values of γ. For values of $\gamma \in (\frac{1}{2}, \infty)$, E diverges at the singularity, decreases to a minimum at a finite radius and then increases to diverge again as r goes to infinity. For values of $\gamma \in (\frac{1}{\sqrt{5}}, \frac{1}{2})$, E goes to zero at the singularity and it has a maximum and a minimum. Whereas for values of $\gamma \in (0, \frac{1}{\sqrt{5}})$, E is monotonically increasing from zero at the singularity to infinite as r goes to infinity.
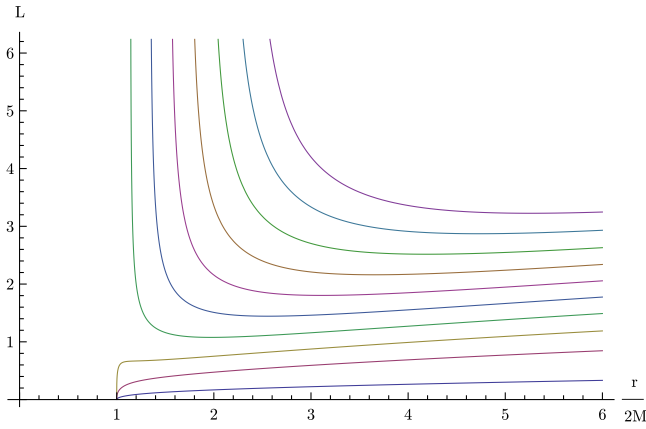
FIG. 9 (color online). The conserved angular momentum per unit mass L is plotted against the radius of the circular orbit r (in units of $\frac{1}{2M}$) for different values of γ. The curves located higher in the diagram correspond to higher values of γ. For values of $\gamma \in (\frac{1}{2}, \infty)$ L diverges at the singularity and as r goes to infinity, thus having a minimum at a finite radius. For values of $\gamma \in (\frac{1}{\sqrt{5}}, \frac{1}{2})$ L has both a minimum and a maximum, goes to zero as r approaches the singularity and diverges as r goes to infinity. Whereas for values of $\gamma \in (0, \frac{1}{\sqrt{5}})$ L is monotonically increasing from zero at the singularity to infinity as r grows indefinitely.

$$r \in (r_{\text{sing}}, \infty). \qquad (44)$$

In Fig. 10 the general behavior of the effective potential for this range of parameter is shown. The effective potential admits only one minimum. Since the potential does not admit maximum, unstable circular orbits do not exist. This is consistent with the existence of stable circular orbits everywhere as discussed above.

The qualitative behavior of the functions $E(r)$ and $L(r)$, as shown in Figs. 8 and 9, is decreasing as the radial coordinate decreases from infinity and vanishes at the singularity.
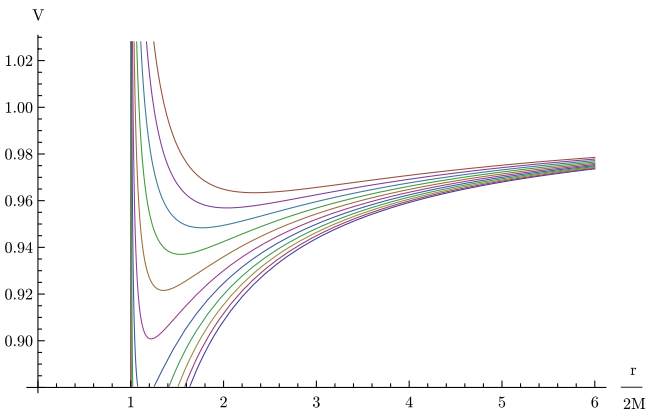

FIG. 10 (color online). The effective potential V is plotted against radial coordinate r in units of $\frac{1}{2M}$ for $\gamma = 0.3 \in (0, \frac{1}{\sqrt{5}})$ for different values of L. The effective potential admits only a minimum implying that unstable orbits in this case do not exist.

2. Case $\gamma \in (\frac{1}{\sqrt{5}}, \frac{1}{2})$

In this range of parameters we get the following relation

$$r_+ > r_- > r_{\text{sing}} > r_{\text{ph}}, \qquad (45)$$

which means that no photon sphere is present in the space-time and there are two distinct regions where circular geodesics can exist, namely

$$r \in (r_+, \infty) \quad \text{and} \quad r \in (r_{\text{sing}}, r_-) \qquad (46)$$

where the first region extends from infinity and the second region extends until to the singularity.

In Fig. 11 we show the general behavior of the effective potential for this range of parameter values. The effective potential admits two minima. These correspond to the two stable circular orbits in the two regions we discussed above. There is also one local maximum between the two minima which lies in the unstable region between the two stable regions.

A particle reaching the innermost stable circular orbit of the outer disk would plunge in towards the singularity until it reaches r_- where stable orbits are allowed again. It would then shock and circularize its motion spiralling towards the singularity.

The qualitative behavior of the energy and angular momentum functions $E(r)$ and $L(r)$ is shown in Figs. 8 and 9. In this case, E and L vanish at the singularity and both have a local maximum and a minimum indicating again that there are two regions where stable circular geodesics can exist. The two regions would correspond to the places where functions decrease with decreasing r, namely, from infinity to first minimum and from the maximum to the singularity. Again the unstable region extends between maximum and minimum, where $E(r)$ and $L(r)$ increase with decreasing r. Since these functions do not blow up at
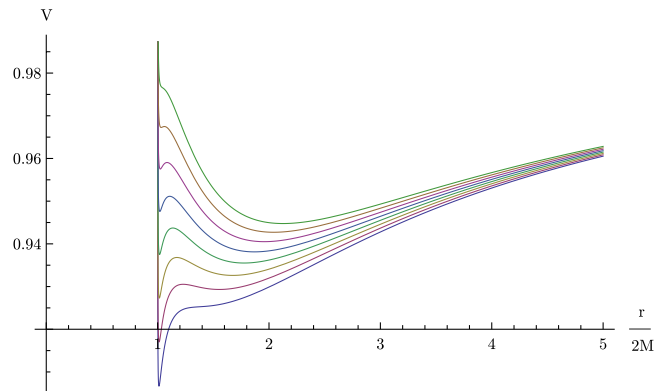

FIG. 11 (color online). The effective potential for radial motion V is plotted as a function of radial coordinate r in units of $\frac{1}{2M}$ for $\gamma = 0.47 \in (\frac{1}{\sqrt{5}}, \frac{1}{2})$ for different values of L. It can be seen that the V admits two minima and one maximum indicating the presence of two regions of stable circular orbits separated by a region of instability.
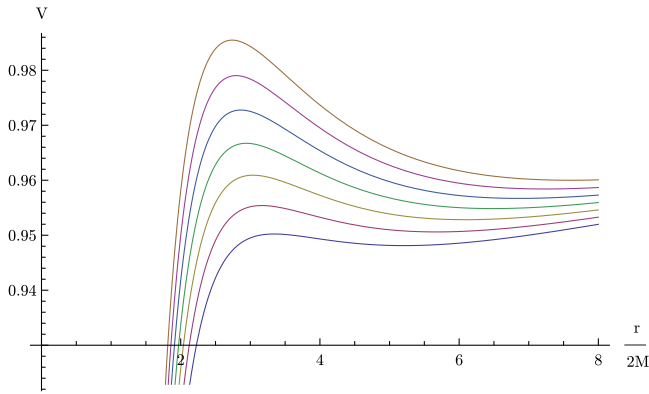
FIG. 12 (color online). The effective potential for radial motion V is plotted as a function of radial coordinate r (in units of $\frac{1}{2M}$) for $\gamma = 1.4 \in (\frac{1}{2}, \infty)$ for different values of L. It can be seen that the V admits one minimum and one maximum, which corresponds to stable and unstable circular orbit, respectively.

any radius we infer that the photon sphere is absent in this case.

3. Case $\gamma \in (\frac{1}{2}, \infty)$

For this range of values of the parameter we have the following relations

$$r_+ > r_{\rm ph} > \max\{r_-, r_{\rm sing}\}, \qquad (47)$$

as can be seen from Fig. 7. Note that r_- can be either larger or smaller than $r_{\rm sing}$ but in both cases lies below the photon sphere. The stable circular orbits can exist in the region

$$r \in (r_+, \infty), \qquad (48)$$

which is above the photon sphere. Unstable circular orbits can exist between the photon sphere and r_+. No circular orbits can exist below the photon sphere until the singularity.

In Fig. 12 we show the general behavior of the effective potential as a function of radius for the parameter in this range. The effective potential admits one maximum and one minimum which correspond to the unstable and stable circular orbits, respectively. The unstable circular orbits lie in the region between the photon sphere and r_+.

The qualitative behavior of the energy and angular momentum functions $E(r)$ and $L(r)$ shows a minimum and it diverges at a certain radius above the singularity corresponding to the photon sphere (see Figs. 8 and 9). This is consistent with the above discussion on the structure of geodesics since as r decreases from infinity, the stable circular geodesics can exist up to the minimum, then unstable orbits exist in the region between the minimum and the radial value where $E(r)$ and $L(r)$ blow up, which is a photon sphere. No circular orbits can exist below the photon sphere.

IV. ACCRETION DISK PROPERTIES

In the context of astrophysics an accretion disk is a nearly flat disk of heated gas whose particles slowly spiral onto a central accreting compact object. Observationally such accretion disks can be detected by their emitted radiation and the spectrum of this radiation can be a valuable source of information about the properties of the accretion disk itself and the central compact object. In the present framework we approximated the accretion disk with an infinitesimally thin disk of test particles moving on circular orbits. The gas is then represented by the test particles moving with angular velocity $\omega = \frac{d\phi}{dt}$ on Keplerian orbits around the central compact object. Then $E(r)$ and $L(r)$ would represent the energy and angular momentum of the test particles circling on the r-orbit of the disk. Then the last stable circular orbits represent the limits within which the disk can exist with the innermost stable circular orbit given by the radius r_+ representing the inner edge of the outer disk. A test particle reaching r_+ would then plunge in free fall until it reaches either the singularity or another radius where stable circular orbits are allowed. The general relativistic setting for accretion disks around a black hole was developed by Novikov and Thorne [14] and by Page and Thorne [15] for steady state accretion on the equatorial plane onto a rotating black hole and it can be extended to the scenarios with naked singularities analyzed here.

Page and Thorne assumed the spacetime to be stationary, axially symmetric, asymptotically flat and reflection symmetric in an equatorial plane. Here both metrics satisfy these requirements once we consider accretion disks on the equatorial plane (note that the JNW metric is spherically symmetric and thus such a choice of the plane is arbitrary while the γ spacetime is axially symmetric and therefore the equatorial plane is fixed). Furthermore the choice of the radial coordinate complies with the requirements imposed in [15] as can be seen from the asymptotic behavior of both metrics and from the fact that r reduces exactly to the radial coordinate of the Schwarzschild metric for $\gamma = 1$ in the γ-metric and to a translation of the Schwarzschild radial coordinate for $\mu = 1$ in the JNW metric.

From the knowledge of the structure equations describing the gas in the disk it is possible to construct the quantities relevant for observations [15]. The radiant energy flux can be written as

$$f(r) = -\frac{\dot{M}_0}{4\pi\sqrt{-\det g}} \frac{\omega_{,r}}{(E - \omega L)^2} \int_{r_+}^{r} (E - \omega L)L_{,r} dr$$

$$(49)$$

where $\dot{M}_0$ is the mass accretion rate and it is assumed to be constant for steady state accretion. Note that since both metrics considered here are continuously linked to the Schwarzschild solution one retrieves precisely the formula
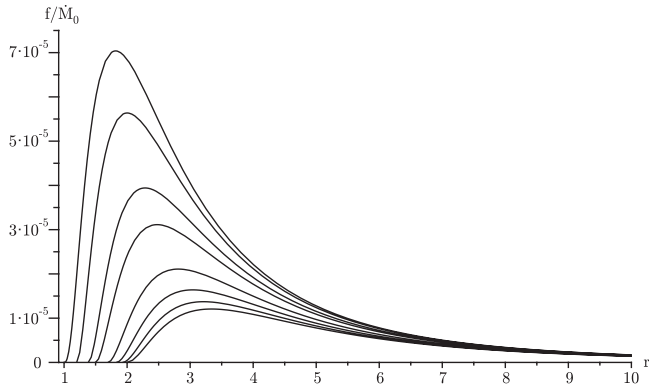
FIG. 13. Radiant energy flux for unit mass accretion rate in natural units for the JNW spacetime with $\mu \leq \sqrt{5}$. Note that the lowest curve represents the flux for the Schwarzschild black hole.

for the radiant energy flux in the Schwarzschild spacetime once the values $\mu = 1$ or $\gamma = 1$ are chosen.

As an example we studied here the qualitative behavior of the radiant energy flux in the JNW metric and in the γ-spacetime in natural units (therefore to obtain the effective flux one would have to reintroduce c and G in the equation), for different values of the parameters μ and γ.

The general feature that emerges for the JNW metric is that when there is an inner boundary for the disk one obtains a flux qualitatively similar but of greater magnitude with respect to that of a black hole (see Fig. 13).

On the other hand, when the accretion disk is allowed to extend up to the singularity the total flux is diverging in the limit of r going to the singularity (see Fig. 14). This divergence of flux in the limit of approach to the singularity is clearly unphysical. Nevertheless, we note here that as the outgoing radiation becomes larger, the outward force acting on the infalling accreting matter will also become bigger. It can be shown that at a particular radius the pressure exerted due to the outgoing radiation will balance out the inward gravitational pull of the gas in the disk.
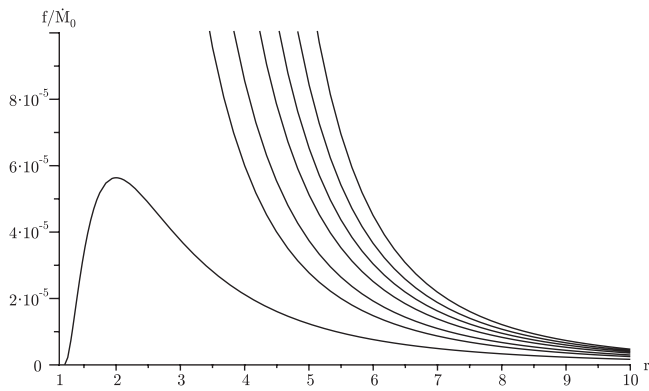

FIG. 14. Radiant energy flux for unit mass accretion rate in natural units for the JNW spacetime with $\mu \geq \sqrt{5}$. Note that the lowest curve represents the case $\mu = \sqrt{5}$, with all values greater than $\sqrt{5}$ diverging as r approaches the singularity.
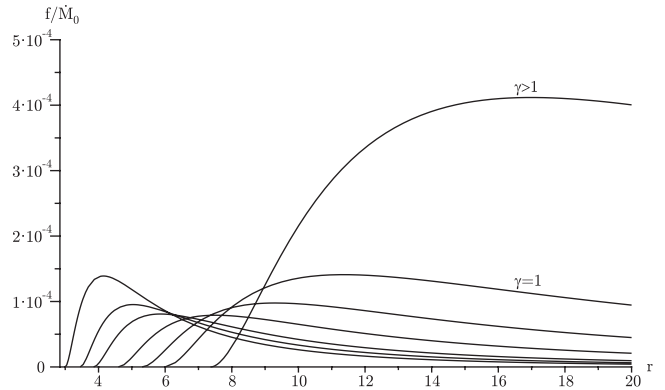

FIG. 15. Radiant energy flux for unit mass accretion rate in natural units for the γ-spacetime with $\gamma \geq 1/2$.

Therefore the accretion disk will not extend below this radius regardless of the presence of a singularity at the center. Thus although the circular geodesics as we have shown in this paper can extend all the way up to the singularity, it is reasonable to expect that physically the accretion disk will be terminated at a finite radius above the singularity. Nevertheless this is a complex issue that is not entirely well understood at present and requires more work and further discussion which is beyond the scope of this paper.

Furthermore, since the γ-metric is not spherically symmetric it should be noted that the axial symmetry will have some influence on the structure of accretion disks close to the singularity. In fact it can be shown that close to the center strong forces in the z direction appear in the spacetime. These forces would disrupt the inflow of particles on the equatorial plane thus deviating them towards the poles, which could be a mechanism that may in principle describe the formation of high energy jets from the poles of such compact objects.

In the case of the γ-metric a similar behavior is found for the radiant energy flux to that of the JNW case. The flux presents a behavior qualitatively similar to that of a black
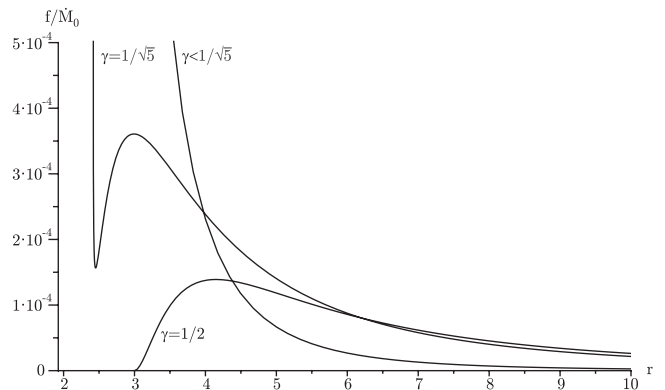

FIG. 16. Radiant energy flux for unit mass accretion rate in natural units for the γ-spacetime with $\gamma \leq 1/2$. Note that the flux diverges for values of $\gamma \leq 1/\sqrt{5}$.

hole when there is an inner edge (see Fig. 15) and diverges in the cases where the accretion disk extends all the way to the singularity (see Fig. 16).

Note that since the total mass as seen by an observer at infinity for the γ-metric is $M\gamma$ it can happen for values of $\gamma < 1$ that the flux is smaller than that of a Schwarzschild black hole with mass M. Nevertheless we expect it to be greater than that of a Schwarzschild black hole with mass $M\gamma$, which would be the right spherical source to compare it with.

To summarize we studied in detail the structure of the circular geodesics in JNW and γ spacetimes in the equatorial plane. JNW and γ-metric are obtained by variation of the Schwarzschild black hole by addition of the massless scalar field and by deformation of spherical symmetry to oblate/prolate spheroidal geometry, respectively. Naively speaking the event horizon in the Schwarzschild black hole transforms into a naked singularity. These solutions are described by two parameters, one related to the mass as in the Schwarzschild case and another related to the scalar charge (μ) or the deformation (γ) and continuously linked to the Schwarzschild spacetime. In fact the Schwarzschild metric is obtained by setting $\mu = 1$ and $\gamma = 1$. The structure of the circular geodesics undergoes a qualitative change as we vary the values of the extra parameter. In both spacetimes the whole range of the parameters can be divided into three regimes.

(i) For $\mu \in (1, 2)$ in JNW metric and for $\gamma \in (\frac{1}{2}, \infty)$ in γ-metric a photon sphere surrounds the singularity and stable circular geodesics can exist from a radius above the photon sphere to infinity. Unstable circular geodesics can exist below this radius up to the photon sphere. No circular geodesics can exist below the photon sphere.

(ii) For $\mu \in (2, \sqrt{5})$ in JNW metric and for $\gamma \in (\frac{1}{\sqrt{5}}, \frac{1}{2})$ in the γ-metric, stable circular geodesics can exist from the singularity to a finite radius and from a larger radius to infinity. There is a region containing unstable circular geodesics between the two stable regions. No photon sphere is present.

(iii) For $\mu \in (\sqrt{5}, \infty)$ in JNW metric and for $\gamma \in (0, \frac{1}{\sqrt{5}})$ in γ-metric, the circular geodesics exist everywhere from the singularity to infinity. Again no photon sphere is present.

This study suggests that there is a significant difference as far as the structure of circular geodesics is concerned in JNW and γ spacetime containing naked singularity as compared to the Schwarzschild black hole, which would reflect into their accretion disk properties.

Similar analysis of circular geodesics in connection with properties of accretion disks around naked singularities have recently drawn some attention as we try to understand the nature of compact objects such as the supermassive ones that exist at the center of galaxies. Harko and Kovacs [7] studied a modified Kerr metric with scalar field

where, due to the presence of the scalar field, a naked singularity is present in the spacetime. They showed that for certain ranges of the parameters, stable circular orbits can exist up to the singularity, a result that does not hold for the Kerr black hole (obtained in the limit of no field).

A similar analysis has been carried out for the Kerr and Reissner-Nordstrom metrics by Pugliese *et al.* [6], where it was shown that for the Kerr naked singularity ($a/M > 1$) unstable circular orbits can extend up to the singularity in some cases, though this does not happen for stable circular orbits. Therefore, an accretion disk made of test particles always extends from a minimum radius to infinity, without any forbidden regions or regions of instability. The disk can be divided into substructures based on whether they consist of corotating and/or counter-rotating particles. For a naked singularity, depending on the value of a/M, the accretion disk may be divided into: (a) two parts—an inner disk with corotating particles and an outer disk with both corotating and counter-rotating particles, (b) three parts, namely, an innermost disk of counter-rotating particles, a second disk of corotating particles and an external disk with both. For a Kerr black hole the allowed region of circular orbits, stable or unstable, terminates outside the horizon. However the accretion disk is similar, extending from a minimum radius to infinity and it can have only two such substructures, a corotating inner disk and an external disk with both kinds of particles; here the size of the inner disk has an upper limit and can even go to zero. In the case (a) for naked singularity, the inner disk has a minimum size but there is no upper limit thus showing that there is some difference in the accretion disk structure between Kerr black hole and Kerr naked singularity. In the Reissner-Nordstrom spacetime a naked singularity is obtained for $Q/M > 1$, where Q is the charge parameter. In this case there exists a forbidden zone outside the horizon or the singularity where no circular orbits are allowed. For the black hole case, the stability region and hence the accretion disk is continuous from a minimum radius to infinity. In the case of a naked singularity, there can be two scenarios depending on the value of Q/M, namely, (a) an accretion disk extending from a minimum radius to infinity, or (b) an accretion disk comprising an inner disk and an outer disk separated by a zone of instability. Therefore the accretion disk structure around a Reissner-Nordstrom naked singularity shows some difference with respect to the black hole case only for a certain range of the parameter.

V. CONCLUDING REMARKS

The study of circular geodesics provides only the first tool to model accretion disks around a compact source. In order to obtain measurable quantities that could eventually be checked against observations, a detailed analysis of the efficiency of conversion of mass of the infalling particles into emitted radiation and the luminosity spectrum of

radiation of the disk are needed. For example assuming that the accretion disk is in thermodynamical equilibrium one can approximate the radiation emitted by the disk with a black body spectrum where the temperature T of the black body is related to the energy flux by $f(r) = \sigma T^4(r)$ (with σ being the Stefan-Boltzmann constant). Then, considering redshift and inclination of the disk with respect to the observer, it is possible to evaluate the observed luminosity spectrum of the black body, which is an observable quantity [7].

It is reasonable to suppose that the pressure of the outgoing radiation near the singularity will be very strong, thus balancing the inflow of particles from the accretion disk. This effect could possibly drive the particles away from the equatorial plane and it should also be analyzed in some detail. Furthermore, electromagnetic fields and possible perpendicular forces that could deviate the particles towards the poles thus creating high energy jets could also be considered.

Nonetheless, the analysis such as given here makes it clear that if naked singularities, which are hypothetical astrophysical objects, do exist in the universe, they would bear an observational signature considerably different from that of a black hole of the same mass. Therefore, it is quite possible that in the foreseeable future we will be able to devise some observational tests to check if such exotic objects are indeed present somewhere in the universe.

ACKNOWLEDGMENTS

[1] P. S. Joshi and I. H. Dwivedi, Phys. Rev. D **47**, 5357 (1993); B. Waugh and K. Lake, Phys. Rev. D **38**, 1315 (1988); D. Christodoulou, Commun. Math. Phys. **93**, 171 (1984); D. M. Eardley and L. Smarr, Phys. Rev. D **19**, 2239 (1979); A. Ori and T. Piran, Phys. Rev. Lett. **59**, 2137 (1987); R. Giamb'o, F. Giannoni, G. Magli, and P. Piccione, Gen. Relativ. Gravit. **36**, 1279 (2004); S. L. Shapiro and S. A. Teukolsky, Phys. Rev. Lett. **66**, 994 (1991); K. Lake, Phys. Rev. D **43**, 1416 (1991); P. S. Joshi, N. Dadhich, and R. Maartens, Phys. Rev. D **65**, 101501 (2002); R. Goswami and P. S. Joshi, Phys. Rev. D **76**, 084026 (2007); T. Harada, H. Iguchi, and K. I. Nakao, Phys. Rev. D **58**, 041502 (1998).

[2] L. Herrera, A. DiPrisco, and E. Fuenmayor, Classical Quantum Gravity **20**, 1125 (2003); P. O. Mazur and E. Mottola, arXiv:gr-qc/0109035v5; M. Visser and D. L. Wiltshire, Classical Quantum Gravity **21**, 1135 (2004); T. Harko, Z. Kovcs, and F. S. N. Lobo, Classical Quantum Gravity **26**, 215006 (2009).

[3] P. S. Joshi, D. Malafarina, and R. Narayan, Classical Quantum Gravity **28**, 235018 (2011).

[4] K. Hioki and K. I. Maeda, Phys. Rev. D **80**, 024042 (2009); K. S. Virbhadra and G. F. R. Ellis, Phys. Rev. D **65**, 103004 (2002); G. N. Gyulchev and S. S. Yazadjiev, Phys. Rev. D **78**, 083004 (2008); K. S. Virbhadra, D. Narasimha, and S. M. Chitre, Astron. Astrophys. **337**, 1 (1998); K. S. Virbhadra and C. R. Keeton, Phys. Rev. D **77**, 124014 (2008); C. Bambi and K. Freese, Phys. Rev. D **79**, 043002 (2009); Z. Stuchlik and J. Schee, Classical Quantum Gravity **27**, 215017 (2010).

[5] C. Bambi and T. Harada, Phys. Rev. D **81**, 104004 (2010); C. Bambi, K. Freese, T. Harada, R. Takahashi, and N. Yoshida, Phys. Rev. D **80**, 104023 (2009); Z. Stuchlik and J. Schee, Classical Quantum Gravity **27**, 215017 (2010).

[6] D. Pugliese, H. Quevedo, and R. Ruffini, Phys. Rev. D **84**, 044030 (2011); **83**, 024021 (2011); **83**, 104052 (2011); P. Pradhan and P. Majumdar, Phys. Lett. A **375**, 474 (2011).

[7] Z. Kovacs and T. Harko, Phys. Rev. D **82**, 124047 (2010).

[8] M. Patil and P. S. Joshi, Phys. Rev. D **84**, 104001 (2011); Classical Quantum Gravity **28**, 235012 (2011); arXiv:1106.5402; M. Patil, P. S. Joshi, K. Nakao, and M. Kimura, arXiv:1108.0288; M. Banados, J. Silk, and S. M. West, Phys. Rev. Lett. **103**, 111102 (2009); M. Banados, B. Hassanain, J. Silk, and S. M. West, Phys. Rev. D **83**, 023004 (2011); A. Williams, Phys. Rev. D **83**, 123004 (2011).

[9] D. M. Zipoy, J. Math. Phys. (N.Y.) **7**, 1137 (1966); B. H. Voorhees, Phys. Rev. D **2**, 2119 (1970).

[10] A. I. Janis, E. T. Newman, and J. Winicour, Phys. Rev. Lett. **20**, 878 (1968).

[11] M. Wyman, Phys. Rev. D **24**, 839 (1981); K. S. Virbhadra, S. Jhingan, and P. S. Joshi, Int. J. Mod. Phys. D **6**, 357 (1997); K. S. Virbhadra, Int. J. Mod. Phys. A **12**, 4831 (1997).

[12] B. Stewart, D. Papadopoulos, L. Witten, R. Berezdivin, and L. Herrera, Gen. Relativ. Gravit. **14**, 97 (1982); L. Herrera, G. Magli, and D. Malafarina, Gen. Relativ. Gravit. **37**, 1371 (2005).

[13] L. Herrera, F. M. Paiva, and N. O. Santos, Int. J. Mod. Phys. D **9**, 649 (2000).

[14] I. D. Novikov and K. S. Thorne, in *Black Holes* edited by C. DeWitt and B. S. DeWitt (Gordon and Breach, New York, 1973), p. 343; N. I. Shakura and R. A. Sunyaev, Astron. Astrophys. **24**, 337 (1973).

[15] D. N. Page and K. S. Thorne, Astrophys. J. **191**, 499 (1974).